Replica-exchange method in van der Waals radius space: Overcoming steric restrictions for biomolecules

Satoru G. Itoh,[a] Hisashi Okumura,[b] and Yuko Okamoto[c]
Department of Physics, School of Science, Nagoya University, Nagoya, Aichi 464-8602, Japan

(Received 5 November 2009; accepted 5 March 2010; published online 5 April 2010)

We present a new type of the Hamiltonian replica-exchange method, where the van der Waals radius parameter and not the temperature is exchanged. By decreasing the van der Waals radii, which control spatial sizes of atoms, this Hamiltonian replica-exchange method overcomes the steric restrictions and energy barriers. Furthermore, the simulation based on this method escapes from the local-minimum free-energy states and realizes effective sampling in the conformational space. We applied this method to an alanine dipeptide in aqueous solution and showed the effectiveness of the method by comparing the results with those obtained from the conventional canonical and replica-exchange methods. © *2010 American Institute of Physics*. [doi:10.1063/1.3372767]

I. INTRODUCTION

Effective samplings in the conformational space by Monte Carlo (MC) and molecular dynamics (MD) simulations are necessary to predict the native structures of proteins. In the conventional canonical-ensemble simulations,[1–6] however, it is difficult to realize effective samplings in complex systems such as proteins. This is because the usual canonical-ensemble simulations tend to get trapped in a few of many local-minimum states. To overcome these difficulties, various generalized-ensemble algorithms have been proposed (for reviews, see, e.g., Refs. 7 and 8).

The replica-exchange method[9] (REM) is one of the most well-known methods among the generalized-ensemble algorithms (see Ref. 10 for the MD version). It is easier to implement than the multicanonical algorithm,[11,12] which is also one of the most well-known generalized-ensemble algorithms (see Refs. 13 and 14 for the MD version), because we do not have to determine a probability weight factor in advance in the REM. In the multicanonical and similar algorithms,[15–24] we employ non-Boltzmann weight factors as the probability weight factors. These non-Boltzmann weight factors are not *a priori* known and have to be determined by tedious procedures. On the other hand, the usual Boltzmann weight factor is employed in REM, and therefore it is not necessary to determine the non-Boltzmann weight factor. The REM uses noninteracting replicas of the target system with different temperatures and realizes a random walk in temperature space by exchanging the temperatures of pairs of replicas. Accordingly, the simulation can avoid getting trapped in local-minimum free-energy states.

For large systems such as proteins in aqueous solution, however, the usual REM has a difficulty. We need to increase the number of replicas in proportion to $O(f^{1/2})$, where f is the number of degrees of freedom.[9] Large biomolecular systems, therefore, require a large number of replicas in the REM and hence huge amount of computation time. In order to overcome this difficulty, it was pointed out that the number of required replicas can be greatly decreased if only the parameter exchanges are performed in the multidimensional REM (MREM) (Ref. 25) without temperature exchanges.[26] In MREM replica exchanges in temperature and/or parameter in the potential energy are performed. MREM is also referred to as the Hamiltonian REM,[26] and in the present article we use the latter terminology.

When we perform simulations of a protein in explicit water solvent, most of the degrees of freedom is occupied by water molecules. In order to predict the native structure of a protein, for instance, we would like to sample effectively the conformational space of the protein rather than water molecules. As an application of the Hamiltonian REM, therefore, Liu *et al.*[27] performed simulations of the peptide in explicit water solvent, in which the scales of the interactions related only to the protein are varied. They could achieve effective samplings in the conformational space of the peptide and save central processing unit cost in comparison with the usual REM. Moreover, other applications of the Hamiltonian REM were reported.[28–30] Kannan and Zacharias[28] focused on the backbone dihedral angles of the peptides and added biasing potential energy to the backbone dihedral angles. They could also achieve effective samplings in this space with the biasing potential energy. However, these biasing potential energy terms are complicated functions and highly dependent on force fields. Affentranger *et al.*[29] also focused on the electrostatic and Lennard-Jones interactions between protein atoms and between protein atoms and solvent atoms. Mu[30] considered only repulsive terms of Lennard-Jones interactions between protein atoms for the Hamiltonian REM. They reduced these interactions by scaling the whole of the relevant terms of the potential energy and realized effective samplings in the conformational space.

In this article, we propose a new type of Hamiltonian REM where we exchange the scaling factor of the van der

[a]Electronic mail: itoh@tb.phys.nagoya-u.ac.jp.
[b]Present Address: Research Center for Computational Science, Institute for Molecular Science, Okazaki, Aichi 444-8585, Japan, Electronic mail: hokumura@ims.ac.jp.
[c]Electronic mail: okamoto@phys.nagoya-u.ac.jp.

Waals radius of solute atoms in the interaction terms among solute atoms only. By reducing this scaling factor, the steric hindrance among solute atoms will be reduced and wide conformational space can be explored. We applied this method to the system of an alanine dipeptide with explicit water molecules and tested the effectiveness of the method by comparing the results with those from the conventional canonical and REMs.

In Sec. II we describe the new Hamiltonian REM. We give the details of the new Hamiltonian REM and canonical simulations that we performed in Sec. III. The results are presented in Sec. IV. Section V is devoted to conclusions.

II. METHODS

A. Hamiltonian REM

We first give a general formulation of the Hamiltonian REM.[25] We consider a system of N atoms with their coordinate vectors and momentum vectors denoted by $q \equiv \{\boldsymbol{q}_1, \cdots, \boldsymbol{q}_N\}$ and $p \equiv \{\boldsymbol{p}_1, \cdots, \boldsymbol{p}_N\}$, respectively. The Hamiltonian H_λ for state $x \equiv (q,p)$ is given by the sum of the kinetic energy K and potential energy E_λ,

$$H_\lambda(x) = K(p) + E_\lambda(q). \tag{1}$$

Here, we are explicitly writing (or introducing) a parameter of interest in the potential energy as λ. In the canonical ensemble at temperature T, each state x is weighted by the Boltzmann factor,

$$W_B(x) = e^{-\beta H_\lambda(x)}, \tag{2}$$

where the inverse temperature β is defined by $\beta = 1/k_B T$ (k_B is Boltzmann's constant).

The generalized ensemble for the Hamiltonian REM consists of M *noninteracting* copies (or, replicas) of the original system in the canonical ensemble at M different parameter values λ_m $(m = 1, \cdots, M)$. We arrange the replicas so that there is always exactly one replica at each λ value. Then there is a one-to-one correspondence between replicas and parameter values; the label i $(i = 1, \cdots, M)$ for replicas is a permutation of the label m $(m = 1, \cdots, M)$ for λ_m, and vice versa,

$$\begin{cases} i = i(m) \equiv f(m), \\ m = m(i) \equiv f^{-1}(i), \end{cases} \tag{3}$$

where $f(m)$ is a permutation function of m and $f^{-1}(i)$ is its inverse.

Let $X = \{x_1^{[i(1)]}, \cdots, x_M^{[i(M)]}\} = \{x_{m(1)}^{[1]}, \cdots, x_{m(M)}^{[M]}\}$ stand for a "state" in this generalized ensemble. Here, the superscript i and the subscript m in $x_m^{[i]}$ label the replica and the parameter, respectively. The state X is specified by the M sets of coordinates $q^{[i]}$ and momenta $p^{[i]}$ of N atoms in replica i at parameter λ_m,

$$x_m^{[i]} \equiv (q^{[i]}, p^{[i]})_m. \tag{4}$$

Because the replicas are noninteracting, the weight factor for the state X in this generalized ensemble is given by the product of Boltzmann factors for each replica i (or at each parameter λ_m),

$$W_{\mathrm{HREM}}(X) = \prod_{i=1}^{M} \exp\{-\beta H_{\lambda_{m(i)}}(x_{m(i)}^{[i]})\} = \prod_{m=1}^{M} \exp\{-\beta H_{\lambda_m}(x_m^{[i(m)]})\}, \tag{5}$$

where $i(m)$ and $m(i)$ are the permutation functions in Eq. (3).

We now consider exchanging a pair of replicas in the generalized ensemble. Suppose we exchange replicas i and j which are at parameter values λ_m and λ_n, respectively,

$$X = \{\cdots, x_m^{[i]}, \cdots, x_n^{[j]}, \cdots\} \to X' = \{\cdots, x_m^{[j]}, \cdots, x_n^{[i]}, \cdots\}. \tag{6}$$

The transition probability for this replica exchange process is given by the usual Metropolis criterion,

$$w(X \to X') = \min\left(1, \frac{W_{\mathrm{HREM}}(X')}{W_{\mathrm{HREM}}(X)}\right) = \min(1, \exp(-\Delta)), \tag{7}$$

where we have[25]

$$\Delta = \beta[(E_{\lambda_m}(q^{[j]}) - E_{\lambda_m}(q^{[i]})) - (E_{\lambda_n}(q^{[j]}) - E_{\lambda_n}(q^{[i]}))]. \tag{8}$$

Here, $q^{[i]}$ and $q^{[j]}$ stand for coordinate vectors for replicas i and j, respectively, before the replica exchange. Note that we need to newly evaluate the potential energy for exchanged coordinates, $E_{\lambda_m}(q^{[j]})$ and $E_{\lambda_n}(q^{[i]})$, because E_{λ_m} and E_{λ_n} are in general different functions. We remark that the kinetic energy terms have canceled out each other in Eq. (8).

The Hamiltonian REM is realized by alternately performing the following two steps.[25]

(1) For each replica, a canonical MC or MD simulation at the corresponding parameter value λ_m is carried out simultaneously and independently for a certain steps with the corresponding Boltzmann factor of Eq. (2) for each replica.
(2) We exchange a pair of replicas i and j which are at the parameter values λ_m and λ_n, respectively. The transition probability for this replica exchange process is given by Eqs. (7) and (8).

Finally, we remark that in order to further enhance sampling, we can always introduce a temperature-exchange process together with the above parameter exchange.[25]

B. van der Waals REM

We now describe our special realization of the Hamiltonian REM, which we refer to as the van der Waals REM (vWREM).

We consider a system consisting of solute molecule(s) in explicit solvent. We can write the total potential energy as follows:

$$E_\lambda(q) = E_p(q_p) + E_{ps}(q_p, q_s) + E_s(q_s), \tag{9}$$

where E_p is the potential energy for the atoms in the solute only, E_{ps} is the interaction term between solute atoms and

solvent atoms, and E_s is the potential energy for the atoms of the solvent molecules only. Here, $q=\{q_p,q_s\}$, where q_p and q_s are the coordinate vectors of the solute atoms and the solvent atoms, respectively, and denoted by $q_p \equiv \{\boldsymbol{q}_1,\cdots,\boldsymbol{q}_{N_p}\}$ and $q_s \equiv \{\boldsymbol{q}_{N_p+1},\cdots,\boldsymbol{q}_N\}$. ($N_p$ is the total number of atoms in the solute.)

We are more concerned with effective sampling of the conformational space of the solute itself than that of the solvent molecules. The steric hindrance of the solute conformations are governed by the van der Waals radii of each atom in the solute. Namely, when the van der Waals radii are large, the solute molecule is bulky and we have more steric hindrance among the solute atoms by the Lennard-Jones interactions, and when it is small, the solute molecule can move more freely. We thus introduce a parameter λ that scales the van der Waals radius of each atom in the solute by

$$\sigma_{k\ell} \to \lambda\sigma_{k\ell}, \tag{10}$$

and write the Lennard-Jones energy term within E_p in Eq. (9) as follows:

$$V_\lambda(q_p) = \sum_{k=1}^{N_p-1} \sum_{\ell=k+1}^{N_p} 4\epsilon_{k\ell}\left\{\left(\frac{\lambda\sigma_{k\ell}}{r_{k\ell}}\right)^{12} - \left(\frac{\lambda\sigma_{k\ell}}{r_{k\ell}}\right)^{6}\right\}, \tag{11}$$

where $r_{k\ell}$ is the distance between atoms k and ℓ in the solute and $\epsilon_{k\ell}$ and $\sigma_{k\ell}$ are the corresponding Lennard-Jones parameters. The original potential energy is recovered when $\lambda=1$, and the steric hindrance of solute conformations is reduced when $\lambda<1$. We remark that this is the only λ-dependent term in E_λ in Eq. (9).

We prepare M values of λ, λ_m $(m=1,\cdots,M)$. Without loss of generality, we can assume that the parameter values are ordered as $\lambda_1<\cdots<\lambda_M$. The vWREM is realized by alternately performing the following two steps.

(1) For each replica, a canonical MC or MD simulation at the corresponding parameter value λ_m is carried out simultaneously and independently for a certain steps with the corresponding Boltzmann factor of Eq. (2) for each replica.

(2) We exchange a pair of replicas i and j which are at the neighboring parameter values λ_m and λ_{m+1}, respectively. The transition probability for this replica exchange process is given by Eq. (7), where Δ in Eq. (8) now reads

$$\Delta = \beta[(V_{\lambda_m}(q_p^{[j]}) - V_{\lambda_m}(q_p^{[i]})) - (V_{\lambda_{m+1}}(q_p^{[j]}) - V_{\lambda_{m+1}}(q_p^{[i]}))]. \tag{12}$$

Here, V_λ is the Lennard-Jones potential energy in Eq. (11) among the solute atoms only.

Note that because the λ dependence of E_λ exists only in V_λ, the rest of the terms have been cancelled out in Eq. (8).

We see that Eq. (12) includes only the coordinates q_p of the atoms in the solute only and is independent of the coordinates q_s of solvent molecules. Because $N_p \ll N$ usually holds, the difficulty in the usual REM that the number of required replicas increases with the number of degrees of freedom is much alleviated in this formalism.

TABLE I. The values of the scaling factor, λ_m $(m=1,\cdots,4)$, of the van der Waals radii in the vWREMD simulation.

Parameter λ_m	Parameter value
λ_1	0.85
λ_2	0.90
λ_3	0.95
λ_4	1.00

C. Reweighting techniques

The results from Hamiltonian REM simulations with different parameter values can be analyzed by the reweighting techniques.[31,32] Suppose that we have carried out a Hamiltonian REM simulation at a constant temperature T_0 with M replicas corresponding to M parameter values λ_m $(m=1,\cdots,M)$.

For appropriate reaction coordinates ξ_1 and ξ_2, the canonical probability distribution $P_{T,\lambda}(\xi_1,\xi_2)$ with any parameter value λ at any temperature T can be calculated from

$$P_{T,\lambda}(\xi_1,\xi_2) = \sum_{E_{\lambda_1},\cdots,E_{\lambda_M}} \frac{\sum_{m=1}^{M}(g_m)^{-1}N_m(E_{\lambda_1},\cdots,E_{\lambda_M};\xi_1,\xi_2)e^{-\beta E_\lambda}}{\sum_{m=1}^{M}(g_m)^{-1}n_m e^{f_{T_0,\lambda_m}-\beta_0 E_{\lambda_m}}}, \tag{13}$$

and

$$e^{-f_{T_0,\lambda_m}} = \sum_{\xi_1,\xi_2} P_{T_0,\lambda_m}(\xi_1,\xi_2). \tag{14}$$

Here, $g_m=1+2\tau_m$, where τ_m is the integrated autocorrelation time with the parameter value λ_m at temperature T_0, $N_m(E_{\lambda_1},\cdots,E_{\lambda_M};\xi_1,\xi_2)$ is the histogram of the M-dimensional energy distributions at the parameter value λ_m and the reaction coordinate values (ξ_1,ξ_2), which was obtained by the Hamiltonian REM simulation, n_m is the total number of samples obtained at the parameter value λ_m. Note that this probability distribution is not normalized. Equations (13) and (14) are solved self-consistently by iteration. For biomolecular systems, the quantity g_m can safely be set to be a constant in the reweighting formulas,[32] and so we set $g_m=1$ throughout the analyses in the present work. Note also that these equations can be easily generalized to any reaction coordinates $(\xi_1,\xi_2,\cdots)$.

From the probability distribution $P_{T,\lambda}(\xi_1,\xi_2)$ in Eq. (13), the expectation value of a physical quantity A with any parameter value λ at any temperature T is given by

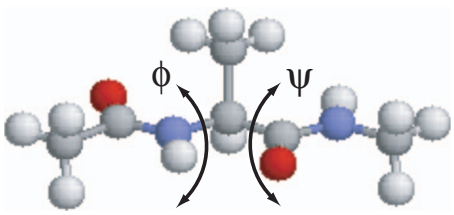

FIG. 1. The common initial conformation of the alanine dipeptide for the present simulations. The figure was created with RasMol (Ref. 41).

TABLE II. Acceptance ratios of replica exchange between pairs of the neighboring parameter values.

Pair of parameter values	Acceptance ratio
$\lambda_1 \leftrightarrow \lambda_2$	0.482
$\lambda_2 \leftrightarrow \lambda_3$	0.540
$\lambda_3 \leftrightarrow \lambda_4$	0.442
$\lambda_4 \leftrightarrow \lambda_1$	0.055

TABLE III. Acceptance ratios of replica exchange between pairs of the neighboring temperatures.

Pair of temperatures	Acceptance ratio
300↔315 K	0.370
315↔335 K	0.269
335↔360 K	0.209
360↔300 K	0.001

$$\langle A \rangle_{T,\lambda} = \frac{\Sigma_{\xi_1,\xi_2} A(\xi_1,\xi_2) P_{T,\lambda}(\xi_1,\xi_2)}{\Sigma_{\xi_1,\xi_2} P_{T,\lambda}(\xi_1,\xi_2)}. \quad (15)$$

We can also calculate the free energy (or, the potential of mean force) as a function of the reaction coordinates ξ_1 and ξ_2 with any parameter value λ at any temperature T from

$$F_{T,\lambda}(\xi_1,\xi_2) = -k_B T \ln P_{T,\lambda}(\xi_1,\xi_2). \quad (16)$$

By utilizing these equations, therefore, we can obtain various physical quantities from the Hamiltonian REM simulations with the original and nonoriginal parameter values. We remark that although we wrote *any* T in Eqs. (13), (15), and (16) above, the valid value T is limited in the vicinity of T_0. We also need the T-exchange process in order to have accurate average quantities for a wide range of T values.

III. COMPUTATIONAL DETAILS

In order to demonstrate the effectiveness of the present Hamiltonian REM, namely, vWREM, in which we exchange pairs of the van der Waals radius parameter values, we applied the vWREM MD algorithm, which we refer to as the *vWREMD*, to the system of an alanine dipeptide in explicit water solvent and compared the results with those obtained by the replica-exchange MD (REMD) simulation and conventional canonical MD simulations. The N-terminus and the C-terminus were blocked by the acetyl group and the N-methyl group, respectively. The number of water molecules was 67. The force field that we adopted was the AMBER parm96 parameter set,[33] and the model for the water molecules was the TIP3P rigid-body model.[34] The vWREMD, REMD, and canonical MD simulations were carried out with the symplectic integrator with rigid-body water molecules, in which the temperature was controlled by the Nosé–Poincaré thermostat.[35–40] The system was put in a cubic unit cell with the side length of 13.4 Å, and we imposed the periodic boundary conditions. Although this system seems to be small, this size is enough to reproduce the experimental results as shown in Ref. 39. The electrostatic potential energy was calculated by the Ewald method, and we employed the minimum image convention for the Lennard-Jones potential energy. The time step was taken to be 0.5 fs.

In the vWREMD simulation, we needed only four replicas ($M=4$). That is, we employed four different parameter values λ_m ($m=1,\cdots,4$). In Table I we list the values of these parameters. These parameters were determined so that exchanges between pairs of replicas were accepted sufficiently as shown in the next section. Therefore, when a different system is employed, we have to adjust these parameters and the number of replicas to realize effective sampling. The original potential energy corresponds to the scale factor $\lambda_4 = 1.0$. The temperature of the system T_0 was set to be 300 K for all the replicas in the vWREMD simulation. We also employed four replicas for the REMD simulation to compare the sampling efficiency with those of the vWREMD simulation, and the four different temperatures were 300, 315, 335, and 360 K, and these temperatures were determined so that exchanges between pairs of replicas were accepted sufficiently. Moreover, we carried out four canonical MD simulations at 300 K, and the difference among these four simu-

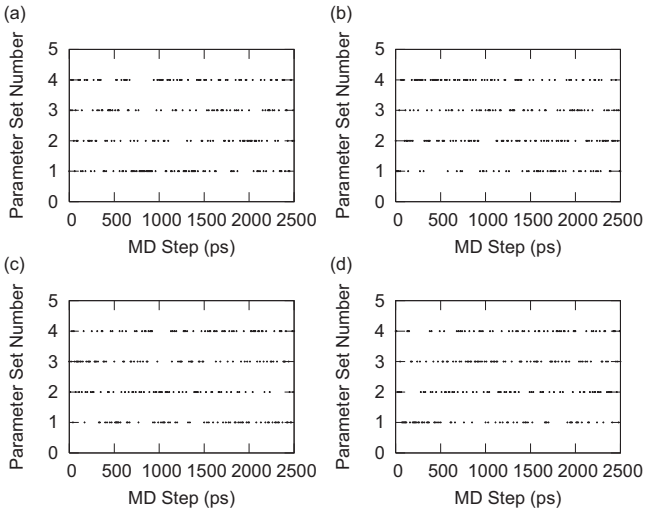

FIG. 2. Time series of the label m of parameter λ_m ($m=1,2,3,4$) in (a) replica 1, (b) replica 2, (c) replica 3, and (d) replica 4 during the vWREMD simulation.

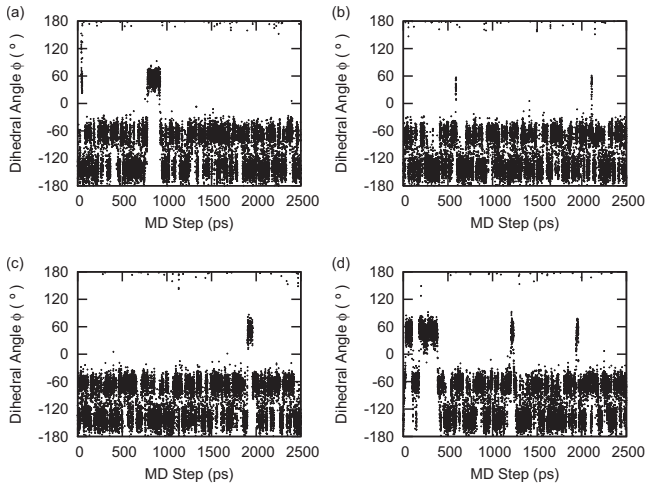

FIG. 3. Time series of the dihedral angle ϕ in (a) replica 1, (b) replica 2, (c) replica 3, and (d) replica 4 during the vWREMD simulation.

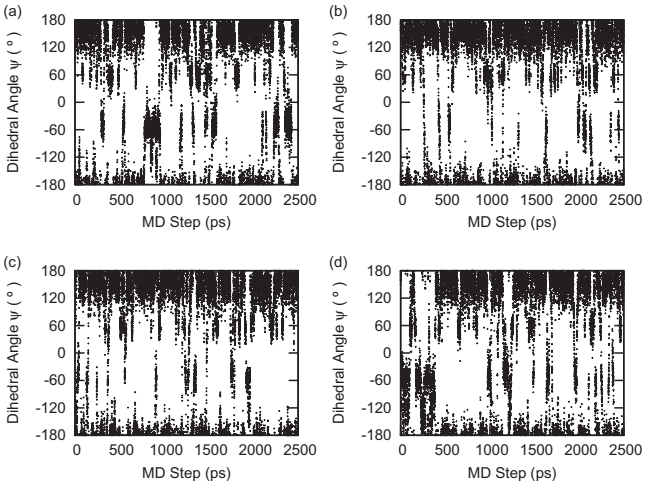

FIG. 4. Time series of the dihedral angle ψ in (a) replica 1, (b) replica 2, (c) replica 3, and (d) replica 4 during the vWREMD simulation.

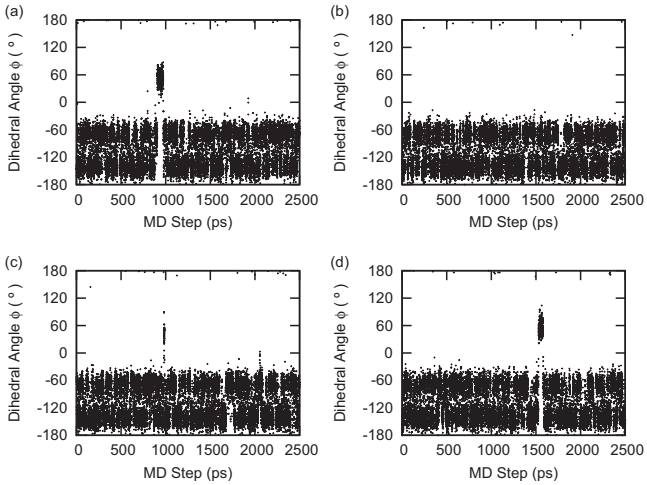

FIG. 6. Time series of the dihedral angle ϕ in (a) replica 1, (b) replica 2, (c) replica 3, and (d) replica 4 during the REMD simulation.

lations was initial velocities. We employed the original parameter value $\lambda=1.0$ for the REMD and canonical MD simulations. The initial conformations were the same for all the simulations, and the initial backbone dihedral angles ϕ and ψ of the alanine dipeptide were set $(\phi,\psi)=(180°,180°)$, as shown in Fig. 1. The total time of the MD simulations were 2.5 ns per replica for the vWREMD and REMD simulations and 2.5 ns for the each canonical simulation, including equilibration for 0.1 ns. The trajectory data were stored every 50 fs. The replica exchange was tried every 250 fs in the vWREMD and REMD simulations.

IV. COMPARISONS OF THE VWREMD SIMULATION WITH THE CANONICAL MD AND REMD SIMULATIONS

We first examine whether the exchanges of pairs of the parameter values were realized sufficiently in our vWREMD simulation. In Table II we list the acceptance ratios of replica exchange of the parameter values in the vWREMD simulation. These acceptance ratios are large enough (>40%) except for the pair of λ_4 and λ_1. Because the difference of these parameter values is much larger than those of other pairs, this low acceptance ratio is expected, and it does not affect the REM performance. Figure 2 shows the time series of the parameter set number m in λ_m which each replica visited. This figure shows that random walks in the parameter space were realized in the vWREMD simulation. In Table III we list the acceptance ratios of replica exchange of the temperatures in the REMD simulation. These acceptance ratios are also large enough, and random walks in the temperature space were sufficiently realized in the REMD simulation.

Figures 3 and 4 show the time series of the backbone-dihedral angles ϕ and ψ for each replica in the vWREMD simulation. Figure 3 indicates that it is difficult to sample the range of the dihedral angle ϕ between 90° and 180°. This is because the steric restriction between the C_β atom of the alanine and the O atom of the acetyl group prevent the rotation in this range. For instance, Fig. 5 is the snapshot of the alanine dipeptide which corresponds to the structure at 2469 ps in replica 3. In this structure, the angle ϕ is 148.8°, and the distance between the C_β atom of the alanine and the O atom of the acetyl group is 2.77 Å. For such a short distance, the two atoms collide with each other. Therefore, the sampling among the range of $90°<\phi<180°$ in the vWREMD simulation was rare, although the scale factor λ_m for the van der Waals radii was lessened. In order to sample this range frequently, it is necessary to employ a much smaller scale factor than the present case. However, confor-

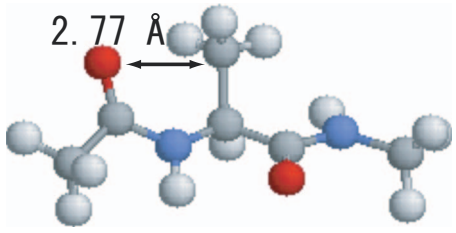

FIG. 5. The snapshot of the alanine dipeptide at 2,469 ps in replica 3 in the vWREMD simulation. The distance between the C_β atom of the alanine and the O atom of the acetyl group is presented. The figure was created with RasMol (Ref. 41).

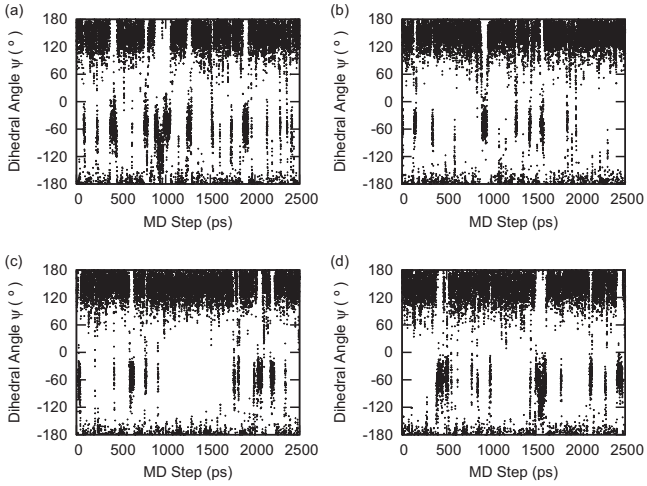

FIG. 7. Time series of the dihedral angle ψ in (a) replica 1, (b) replica 2, (c) replica 3, and (d) replica 4 during the REMD simulation.

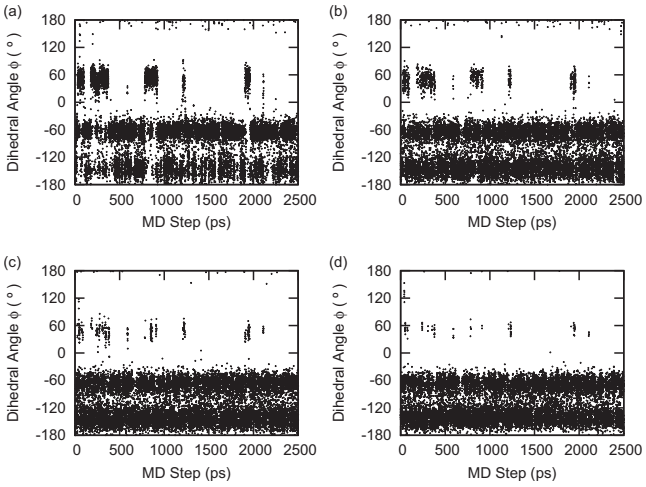

FIG. 8. Time series of the dihedral angle ϕ with the parameter values (a) λ_1, (b) λ_2, (c) λ_3, and (d) λ_4 during the vWREMD simulation.

mations among this range have quite high potential energy due to the collisions between the C_β atom of the alanine and the O atom of the acetyl group, and it is not so important to sample this range at room temperature. On the other hand, the vWREMD simulation realized effective samplings with respect to ψ in all the replicas, as shown in Fig. 4. This is because the van der Waals radius of the H atom of the N-methyl group that has the covalent bond with the N atom of the N-methyl group is small, and steric restrictions between the C_β atom of the alanine and the H atom are less than those between the C_β atom of the alanine and the O atom of the acetyl group.

Figures 6 and 7 show the time series of the backbone-dihedral angles ϕ and ψ for each replica in the REMD simulation. From these figures, it is also difficult to sample the range of the dihedral angle ϕ between 90° and 180° in the REMD simulation. Furthermore, samplings in the ϕ space in the vWREMD simulation were more effective than those in the REMD simulation (compare Fig. 3 with Fig. 6), although the effectiveness of samplings in the ψ space was not so different between the two simulations (compare Fig. 4 with Fig. 7).

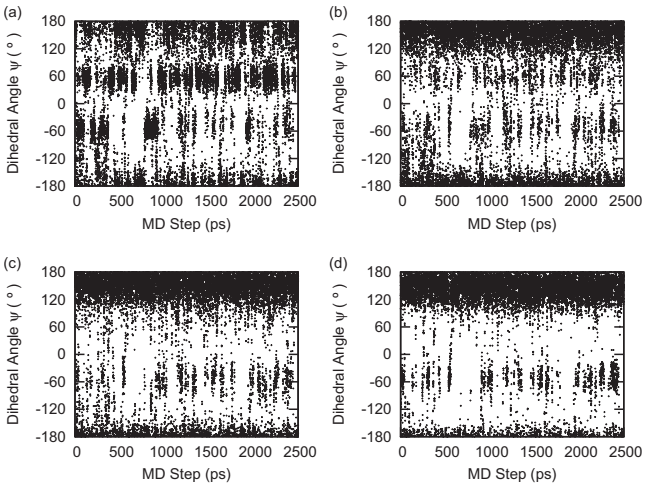

FIG. 9. Time series of the dihedral angle ψ with the parameter values (a) λ_1, (b) λ_2, (c) λ_3, and (d) λ_4 during the vWREMD simulation.

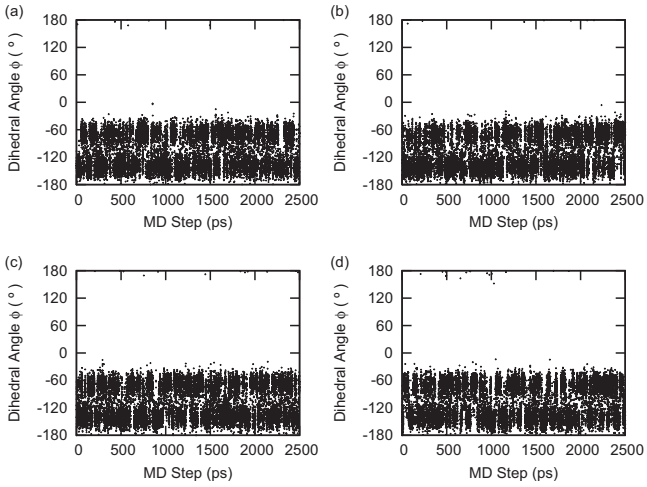

FIG. 10. Time series of the dihedral angle ϕ during the conventional canonical MD simulations. (a)–(d) were obtained with different initial velocities.

Figures 8 and 9 show the time series of the backbone-dihedral angles ϕ and ψ for each parameter value. These figures show that the smaller the scale factor λ_m of the van der Waals radii is, the more efficient the sampling in the backbone-dihedral-angle space is. This is because the steric restrictions are reduced by lessening the scale factor and the energy barriers caused by the steric restrictions are decreased. For comparisons, we also show those from the four conventional canonical MD simulations with the original parameter value of $\lambda=1$ in Figs. 10 and 11. Comparing Fig. 8(d) with Figs. 10(a)–10(d) and Fig. 9(d) with Figs. 11(a)–11(d), the vWREMD with the original parameter value λ_4 (=1) sampled the dihedral-angle space more effectively than the usual canonical MD simulations and did not get trapped in the local-minimum free-energy states. In other words, the canonical MD simulations with the original parameter value could not overcome energy barriers caused by the steric restrictions and got trapped in the local-minimum free-energy states. Therefore, effective samplings in the dihedral-angle space cannot be realized in the usual canonical MD simulations.

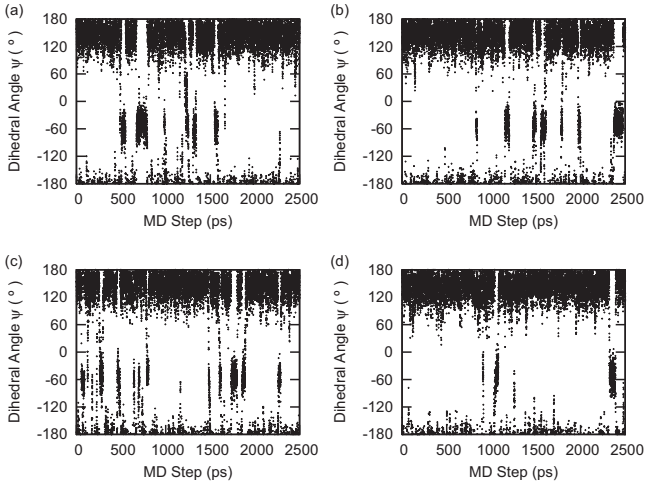

FIG. 11. Time series of the dihedral angle ψ during the conventional canonical MD simulations. (a)–(d) were obtained with different initial velocities.

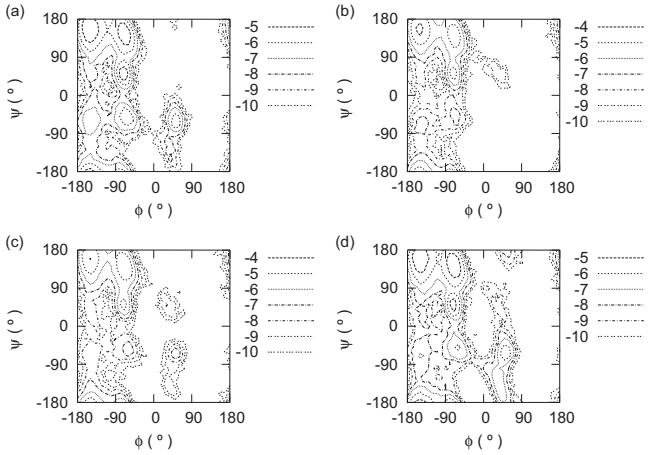

FIG. 12. The logarithm of the probability distribution ln $P(\phi,\psi)$ with respect to the dihedral angles ϕ and ψ for (a) replica 1, (b) replica 2, (c) replica 3, and (d) replica 4 in the vWREMD simulation.

The logarithm of the probability distributions, ln $P(\phi,\psi)$, with respect to dihedral angles ϕ and ψ were obtained from the vWREMD simulations. Figures 12 and 13 show ln $P(\phi,\psi)$ for each replica and those for each parameter value, respectively. From Fig. 12 there are two regions in the vicinites of $(\phi,\psi)=(0°,0°)$ and $(\phi,\psi)=(0°,180°)$ in which the samplings were rare (in addition to the range of $90°<\phi<180°$). This is because in the vicinity of $(\phi,\psi)=(0°,0°)$, the O atom of the acetyl group and the H atom of N-methyl group collide with each other as in a structure shown in Fig. 14(a). In the region of the neighborhood of $(\phi,\psi)=(0°,180°)$, the O atom of the acetyl group and the O atom of the alanine also collide as in a structure shown in Fig. 14(b). It is obvious that steric restrictions in these regions were reduced and that the energy barriers were decreased by decreasing the scale factor as shown in Fig. 13. However, the effects of reducing energy barriers around $(\phi,\psi)=(0°,180°)$ are less than those around $(\phi,\psi)=(0°,0°)$. This is because the O atom of the acetyl group and the O atom of the alanine have negative charges, and repulsive forces caused by these charges act on both atoms.

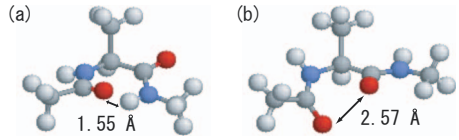

FIG. 14. (a) The snapshot of the alanine dipeptide at 895.55 ps in replica 1 in the vWREMD simulation. The structure has backbone-dihedral angles of $(\phi,\psi)=(15.5°,5.2°)$. The distance between the O atom of the acetyl group and the H atom of N-methyl group is given. (b) The snapshot of the alanine dipeptide at 2465.65 ps in replica 1 in the vWREMD simulation. The structure has backbone-dihedral angles of $(\phi,\psi)=(-27.7°,174.1°)$. The distance between the O atom of the acetyl group and the O atom of the alanine is given. The figures were created with RasMol (Ref. 41).

Therefore, by reducing the atomic charges as well as the van der Waals radii, more effective sampling may be realized in the conformational space.

Figure 15 show ln $P(\phi,\psi)$ at each temperature obtained from the REMD simulation. The effective samplings were realized at higher temperatures than lower temperatures from this figure. This is because simulations could overcome the potential energy barriers at the higher temperatures. However, the efficiency of samplings in the vWREMD simulation was better than the REMD simulation as mentioned above (compare Fig. 13 with Fig. 15).

Figure 16 shows the free-energy landscapes at $T_0=300$ K with respect to the backbone-dihedral angles ϕ and ψ with the original parameter value ($\lambda=1$). The free-energy landscape in Fig. 16(a) was calculated from Eq. (16) by the reweighting techniques in Eqs. (13) and (14). The free-energy landscape in Fig. 16(b) was obtained from the raw histogram with the original parameter value λ_4 in the vWREMD simulation. The average of the raw histograms of the four canonical MD simulations was employed to calculate the free-energy landscape in Fig. 16(c). The free-energy landscape of the conventional canonical MD simulations is inaccurate due to insufficient sampling in the backbone-dihedral-angle space as shown in Figs. 10 and 11. The free-energy landscape obtained by the reweighting techniques in Fig. 16(a) shows a better statistics even at free-energy barriers among the local-minimum states in comparison with that obtained from the raw histogram in Fig. 16(b). This is be-

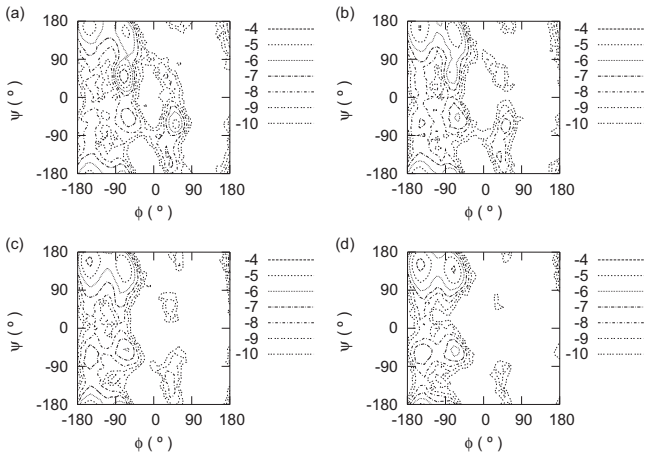

FIG. 13. The logarithm of the probability distribution ln $P(\phi,\psi)$ with respect to the dihedral angles ϕ and ψ with parameter values (a) λ_1, (b) λ_2, (c) λ_3, and (d) λ_4 in the vWREMD simulation.

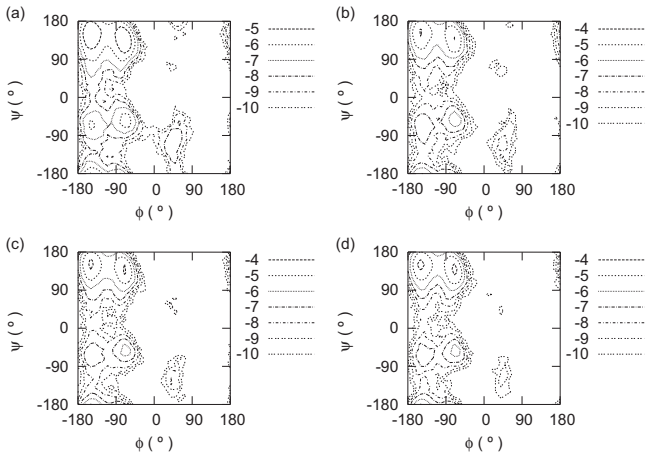

FIG. 15. The logarithm of the probability distribution ln $P(\phi,\psi)$ with respect to the dihedral angles ϕ and ψ at (a) 360 K, (b) 335 K, (c) 315 K, and (d) 300 K in the REMD simulation.

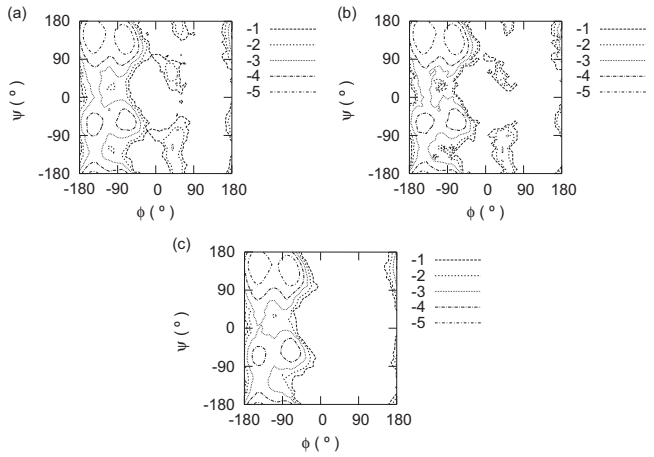

FIG. 16. The free-energy landscapes at T_0=300 K with respect to the backbone-dihedral angles ϕ and ψ with the original parameter value $\lambda=1$. These were obtained from (a) the reweighting techniques applied to the results of the vWREMD simulation, (b) the raw histogram with the original parameter value λ_4 in the vWREMD simulation, and (c) the raw histogram in the canonical MD simulations.

cause the information of all the other parameter values can be reflected by the reweighting techniques. Therefore, more accurate free-energy landscape can be obtained by the reweighting techniques.

V. CONCLUSIONS

In this article, we introduced a new type of Hamiltonian REM, the vWREM in which the scale factor of the van der Waals radii of the solute atoms is exchanged only in the Lennard-Jones interactions among themselves. The steric hindrance due to the Lennard-Jones repulsions can be reduced by this method. Accordingly, the vWREM simulation can realize effective sampling in the backbone-dihedral-angle space without getting trapped in local-minimum free-energy states in comparison with the conventional canonical MD simulations. We also showed that the efficiency of samplings in the vWREM simulation is better than those in the REMD simulation with the same number of replicas. Employing the reweighting techniques, furthermore, we can obtain accurate free-energy landscape.

Although we considered only exchanges of the scale factor of the van der Waals radii in this article, this idea can be extended to other parameters. For example, the scale factor of partial charges of solute atoms can also be introduced and exchanged so that we can also realize even more efficient sampling in the conformational space. The generalization of the formalism in Sec. II to other parameters is straightforward including the reweighting techniques. Moreover, these formalisms are independent of the degrees of freedom of solvent molecules. Therefore, these algorithms can be easily applied to large biomolecular systems.

ACKNOWLEDGMENTS

The computations were performed on the computers at the Research Center for Computational Science, Institute for Molecular Science. This work was supported, in part, by Grants-in-Aid for Scientific Research on Innovative Areas ("Fluctuations and Biological Functions") and for the Next-Generation Super Computing Project, Nanoscience Program from the Ministry of Education, Culture, Sports, Science and Technology (MEXT), Japan.

[1] N. Metropolis, A. W. Rosenbluth, M. N. Rosenbluth, A. H. Teller, and E. Teller, J. Chem. Phys. **21**, 1087 (1953).
[2] W. G. Hoover, A. J. C. Ladd, and B. Moran, Phys. Rev. Lett. **48**, 1818 (1982).
[3] D. J. Evans, J. Chem. Phys. **78**, 3297 (1983).
[4] S. Nosé, Mol. Phys. **52**, 255 (1984).
[5] S. Nosé, J. Chem. Phys. **81**, 511 (1984).
[6] W. G. Hoover, Phys. Rev. A **31**, 1695 (1985).
[7] A. Mitsutake, Y. Sugita, and Y. Okamoto, Biopolymers **60**, 96 (2001).
[8] S. G. Itoh, H. Okumura, and Y. Okamoto, Mol. Simul. **33**, 47 (2007).
[9] K. Hukushima and K. Nemoto, J. Phys. Soc. Jpn. **65**, 1604 (1996).
[10] Y. Sugita and Y. Okamoto, Chem. Phys. Lett. **314**, 141 (1999).
[11] B. A. Berg and T. Neuhaus, Phys. Lett. B **267**, 249 (1991).
[12] B. A. Berg and T. Neuhaus, Phys. Rev. Lett. **68**, 9 (1992).
[13] U. H. E. Hansmann, Y. Okamoto, and F. Eisenmenger, Chem. Phys. Lett. **259**, 321 (1996).
[14] N. Nakajima, H. Nakamura, and A. Kidera, J. Phys. Chem. B **101**, 817 (1997).
[15] H. Okumura and Y. Okamoto, Chem. Phys. Lett. **383**, 391 (2004).
[16] H. Okumura and Y. Okamoto, Phys. Rev. E **70**, 026702 (2004).
[17] H. Okumura and Y. Okamoto, J. Phys. Soc. Jpn. **73**, 3304 (2004).
[18] H. Okumura and Y. Okamoto, Chem. Phys. Lett. **391**, 248 (2004).
[19] H. Okumura and Y. Okamoto, J. Comput. Chem. **27**, 379 (2006).
[20] B. A. Berg, H. Noguchi, and Y. Okamoto, Phys. Rev. E **68**, 036126 (2003).
[21] S. G. Itoh and Y. Okamoto, Chem. Phys. Lett. **400**, 308 (2004).
[22] S. G. Itoh and Y. Okamoto, J. Chem. Phys. **124**, 104103 (2006).
[23] S. G. Itoh and Y. Okamoto, Mol. Simul. **33**, 83 (2007).
[24] S. G. Itoh and Y. Okamoto, Phys. Rev. E **76**, 026705 (2007).
[25] Y. Sugita, A. Kitao, and Y. Okamoto, J. Chem. Phys. **113**, 6042 (2000).
[26] H. Fukunishi, O. Watanabe, and S. Takada, J. Chem. Phys. **116**, 9058 (2002).
[27] P. Liu, B. Kim, R. A. Friesner, and B. J. Berne, Proc. Natl. Acad. Sci. U.S.A. **102**, 13749 (2005).
[28] S. Kannan and M. Zacharias, Proteins **66**, 697 (2007).
[29] R. Affentranger, I. Tavernelli, and E. E. Di Iorio, J. Chem. Theory Comput. **2**, 217 (2006).
[30] Y. Mu, J. Chem. Phys. **130**, 164107 (2009).
[31] A. M. Ferrenberg and R. H. Swendsen, Phys. Rev. Lett. **63**, 1195 (1989).
[32] S. Kumar, D. Bouzida, R. H. Swendsen, P. A. Kollman, and J. M. Rosenberg, J. Comput. Chem. **13**, 1011 (1992).
[33] P. A. Kollman, R. Dixon, W. Cornell, T. Fox, C. Chipot, and A. Pohorille, in *Computer Simulation of Biomolecular Systems*, edited by A. Wilkinson, P. Weiner, and W. F. van Gunsteren (Elsevier, Dordrecht, 1997), Vol. 3, p. 83.
[34] W. L. Jorgensen, J. Chandrasekhar, J. D. Madura, R. W. Impey, and M. L. Klein, J. Chem. Phys. **79**, 926 (1983).
[35] S. D. Bond, B. J. Leimkuhler, and B. B. Laird, J. Comput. Phys. **151**, 114 (1999).
[36] S. Nosé, J. Phys. Soc. Jpn. **70**, 75 (2001).
[37] H. Okumura, S. G. Itoh, and Y. Okamoto, J. Chem. Phys. **126**, 084103 (2007).
[38] H. Okumura and Y. Okamoto, Bull. Chem. Soc. Jpn. **80**, 1114 (2007).
[39] H. Okumura and Y. Okamoto, J. Phys. Chem. B **112**, 12038 (2008).
[40] H. Okumura, J. Chem. Phys. **129**, 124116 (2008).
[41] R. A. Sayle and E. J. Milner-White, Trends Biochem. Sci. **20**, 374 (1995).